Gap-Leaping Western Boundary Current in a Circular Tank Model

VITALII A. SHEREMET AND JOSEPH KUEHL

Graduate School of Oceanography, University of Rhode Island, Narragansett, Rhode Island

(Manuscript received 14 September 2005, in final form 10 July 2006)

ABSTRACT

An oceanographically generic problem of the interaction of a boundary current with bathymetric features such as a gap in the ridge or a strait between two islands is considered. Multiple flow patterns (penetrating or leaping the gap) and hysteresis (dependence on prior evolution) may exist in such systems. Examples include the Gulf Stream leaping from the Yucatan to Florida and the Kuroshio leaping from Luzon to Taiwan. Using numerical analysis, Sheremet earlier found that multiple steady states can be explained by variation in the balance between the inertia (which promotes leaping state) and the β effect (which promotes penetrating state). In the present work a verification of the multiple states and hysteresis in a laboratory model are offered. To set up a gap-leaping current, a circular tank with a sloping bottom (simulating the β effect) is used, and the flow is driven using a new method of pumping fluid through sponges (thus generating a Sverdrup flow in the interior). A semicircular ridge with a gap is inserted into the western part of the tank. Using a dye release flow visualization method, the existence of multiple flow patterns over varying boundary current transport values differing by a factor of more than 2 are dramatically shown. An associated numerical model in bipolar curvilinear coordinates, which allows for the matching of all the boundaries, reproduces the laboratory results very well. This idealized problem offers a very useful geophysical test case for numerical models involving flow separation and reattachment.

1. Introduction

The interaction of a boundary current with bathymetric features such as a gap in the ridge or a strait between two islands is an important and interesting oceanographic problem. Examples include western boundary currents such as the Gulf Stream leaping from the Yucatan to Florida or the Kuroshio leaping from Luzon to Taiwan and shelfbreak currents such as the one leaping from the Scotian shelf to Georges Bank (Cho et al. 2002; the so-called Scotian Shelf Water crossover event). Multiple flow patterns (when flow either leaps across or penetrates through the gap forming a loop current and shedding rings) are known to exist in such systems. A number of theoretical works have been devoted to explaining various aspects of gap flow dynamics (e.g., Nof and Olson 1983; Simmons and Nof 2002; Johnson and McDonald 2004). Recently Sheremet (2001) considered a gap-leaping problem in the context of a western boundary current and, by using numerical analysis, found that the multiple steady states can be explained by variation in the balance between the inertia (which promotes the leaping state) and the β effect (which promotes the penetrating state). Moreover, it was found that in transition from one type of flow to another a hysteresis exists: the flow state depends on prior evolution and two different flow states are possible for exactly the same external governing conditions.

It is known that numerical methods sometimes exhibit spurious behavior, especially in the presence of sharp features in the boundary; for example, the notorious problem of the Gulf Stream separation from Cape Hatteras: certain ocean circulation models fail to properly represent separation and allow the current to hug the coast. To dismiss such a possibility we felt compelled to demonstrate the existence of multiple steady states and hysteresis in the gap-leaping problem using a laboratory model and thus confirm our earlier numerical findings.

In (Sheremet 2001) the western boundary current was assumed to be infinitely long, which is impossible to produce in the laboratory experiments. Instead we built

Corresponding author address: V. A. Sheremet, Graduate School of Oceanography, University of Rhode Island, Narragansett, RI 02882.
E-mail: vsheremet@gso.uri.edu

DOI: 10.1175/JPO3069.1

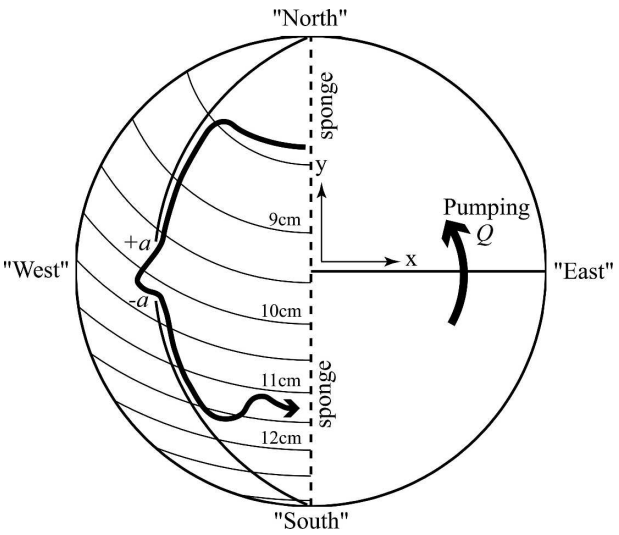

FIG. 1. Sketch of the laboratory experiment. In the working area ($x < 0$) shown by thin circular lines are the depth (geostrophic) contours for a solid body rotation state, $H_0 = 10$ cm.

a laboratory model in a circular tank and developed a numerical model that matches it as accurately as possible. To set up a gap-leaping current we use a circular tank with a sloping bottom (simulating the β effect). Traditionally in experiments simulating ocean circulation the flow was generated by a lid rotating at a slightly different angular velocity than the tank (Pedlosky and Greenspan 1967). Here we drive the flow using a new method of pumping fluid through sponges (thus generating a Sverdrup flow in the interior). The laboratory model is explained in detail in section 2. The mathematical formulation of the problem is presented in section 3 while details of the associated numerical model in curvilinear coordinates are discussed in the appendix. We use a bipolar coordinate system in order to accommodate a circular geometry of the tank and the ridge inside it. The results of the laboratory experiments along with the matching numerical solutions are shown in section 4. The last section presents the conclusions.

2. Laboratory model

The laboratory apparatus consists of a circular tank with a radius of $R = 48.7$ cm, which is placed in the center of a rotating table. The tank is divided into several compartments (Fig. 1). We introduce Cartesian coordinates (x, y) with the origin being at the center of the tank, x pointing "east" (right of the figure), and y pointing "north" (top of the figure). The analogs of geographic east, west, north, and south will become clear below. The "western" semicircle ($x < 0$) is a working area where the circulation is supposed to mimic the subtropical gyre, it is separated from the "eastern" semicircle ($x > 0$) by a sponge wall. The eastern semicircle is in turn divided by a solid barrier into the "northern" ($y > 0$) and "southern" ($y < 0$) sectors. The flow is driven by pumping water from the southern into the northern sector, lowering pressure in the former and raising it in the latter relative to the western compartment. As a consequence water starts to percolate through the sponges generating circulation in the working area.

The western compartment has a bottom with slope, $S = 0.05$ from north to south, in order to produce the β effect. In a solid body rotation the surface of fluid assumes the shape of a paraboloid, hence the total depth of the fluid layer $H(x, y)$ in the working area is

$$H(x, y) = H_0 - Sy + \frac{1}{2}\frac{\Omega^2}{g}\left(r^2 - \frac{1}{2}R^2\right), \qquad (1)$$

where H_0 is the depth at the center of the tank in the nonrotating state, $\Omega = 1\ \mathrm{s}^{-1}$ is the rotation rate of the table, $r = (x^2 + y^2)^{1/2}$ is the radius, and $g = 980.3\ \mathrm{cm\ s}^{-2}$ is the gravitational acceleration. The last term $(\frac{1}{2})R^2$ in (1) takes into account conservation of mass between the rotating and nonrotating states. The potential vorticity $q(x, y) = 2\Omega/H(x, y)$ is constant along geostrophic contours that have circular shapes by virtue of (1); they originate at the eastern boundary (the sponge wall $x = 0$), curve "northward," and impinge on the circumference of the tank ($r = R$) (Fig. 1). Because the fluid layer becomes shallower and hence the potential vorticity increases northward, the topographic Rossby waves in the tank would propagate "westward" in analogy to the planetary Rossby waves in the ocean.

Inserted within the working area is a narrow vertical impermeable ridge having a circular shape and passing through the points $(x, y) = (0, -R)$; $(-2R/3, 0)$; $(0, R)$. In the middle the ridge has a gap of half-width a extending all the way to the bottom. When the pump is on, the flow incoming through the northern sponge ($x = 0$, $y > 0$) follows geostrophic contours, according to the Sverdrupian dynamics, until it impinges on the ridge and forms a western boundary current carrying water south along the ridge (Sverdrup 1947; Stommel 1948). Depending on the governing parameters, the boundary current can either leap across the gap for relatively strong inertia or in the case of weak inertia penetrate through the gap as a loop current pushed farther westward by the β effect (Sheremet 2001). Upon negotiating the gap the boundary current continues south along the ridge gradually feeding the east-

ward outflow, which follows the geostrophic contours back to the eastern boundary where its is sucked through the sponge ($x = 0$, $y < 0$).

Since pumping raises or lowers the pressure uniformly over the eastern sectors the inlet $u(0, y) = U_1$ ($0 < y < R$) and outlet $u(0, y) = U_2$ ($-R < y < 0$) velocities are uniform as well, except near the boundaries ($y = 0, \pm 1$), provided that the sponges have uniform thickness. This was checked by rapidly adding and mixing dye in the source eastern sector and observing a straight dyed water front appearing and propagating away from the sponge in the working compartment. The constants U_1 and U_2 are constrained by the condition

$$U_1 \int_0^R H(0, y)\, dy = -U_2 \int_{-R}^0 H(0, y)\, dy = Q, \quad (2)$$

where Q is the volume pumping rate.

When the slope of the bottom is adjusted ($S = 0.05$) to match that of the free surface at the northern end ($x = 0$, $y = R$),

$$S = \frac{\Omega^2 R}{g}, \quad (3)$$

the potential vorticity gradient vanishes there,

$$\partial H(x, y)/\partial y = 0; \quad (4)$$

also this point is a common center of all circular geostrophic contours [e.g., (1)]. In this way we can generate a western boundary current with nearly constant potential vorticity at its origin. There is a lot of evidence that oceanic western boundary currents have this property. In case of the Kuroshio in the western Pacific, Toole et al. (1990) measured that in the latitude range from 8° to 18°N the potential vorticity of the surface layer above the main thermocline is practically a constant 1×10^{-7} m^{-1} s^{-1} with the accuracy better than 10%. We also note that the Kuroshio flows northward while in the laboratory experiment we model it by a southward-flowing boundary current. We do so in order to take advantage of nearly uniform potential vorticity in the northern part of the tank and also in order to have a longer span for the boundary current to travel once it formed since the geostrophic contours bend north.

3. Mathematical formulation

Though in the laboratory the ratio of vertical to horizontal scales is not very small, the shallow-water equations can still be used because the rapid rotation of the fluid suppresses the vertical shear of velocity except in the Ekman bottom boundary layer of thickness $h_E = (\nu/\Omega)^{1/2}$, where ν is the kinematic viscosity of water. Furthermore, the Ekman layer correction decays exponentially fast outside the boundary layer. This is justified, if for the typical horizontal velocity U, the Rossby number $\mathrm{Ro} = U/(2\Omega R)$ is small. Then for the flow outside the Ekman layer the Navier–Stokes equations can be written only in terms of horizontal components of velocity $\mathbf{u} = (u, v)$ independent of vertical coordinate z. And these equations can be regarded to be exact as far as the expansion in Ro is concerned. The horizontal momentum equations in a Gromeka–Lamb vector form[1] are

$$\mathbf{u}_t + \nabla(p + e) + (2\Omega + \omega)\mathbf{k} \times \mathbf{u} = \nu\nabla^2\mathbf{u}, \quad (5)$$

and the continuity equation is

$$\frac{1}{g} p_t + \mathrm{div}(\mathbf{u}H) + \mathrm{div}\boldsymbol{\Pi}_E = 0. \quad (6)$$

The subscript t indicates differentiation with respect to time; ∇, rot, div are the vector operators involving only horizontal derivatives; p is the pressure anomaly relative to a solid body rotation state divided by uniform density of water; $\mathbf{k}$ is the vertical unit vector; e is the kinetic energy divided by density of water; and $\omega = \mathrm{rot}\mathbf{u}$ is the vertical component of relative vorticity. According to the linear Ekman (1905) theory for a rapidly rotating fluid the flow divergence in the bottom boundary layer can be expressed in terms of the ambient relative vorticity:

$$\mathrm{div}\boldsymbol{\Pi}_E = -\frac{1}{2} h_E \omega. \quad (7)$$

This expression gives the first-order contribution of vertical viscosity to dissipation, which is also called Ekman suction. More subtle details, such as the three-dimensional structure of the flow near lateral boundaries, can be found in (Pedlosky 1968). We neglect the contribution of the pressure anomaly to the total layer depth, therefore (6) is linear.

To advance a theoretical analysis it is convenient to reduce the problem to the streamfunction–vorticity formulation as in (Zavala Sanson and van Heijst 2002). For comparison with our laboratory experiments (which usually showed steady flow patterns except during the transient phase) we are mostly interested in steady solutions. Neglecting the evolutionary term in (6) allows us to introduce the function of total transport

[1] Professor I. S. Gromeka (1851–89) was a distinguished Russian physicist on the faculty at Imperial Kazan University and was known for his fundamental works in hydromechanics—in particular, Gromeka (1885).

ψ, which combines the transport in the inviscid interior and the transport in the Ekman layer:

$$H\mathbf{u} + \frac{1}{2}h_E\mathbf{k}\times\mathbf{u} = \mathbf{k}\times\nabla\psi. \tag{8}$$

Expanding (8) in h_E/H [$O(10^{-2})$ in the experiments] and keeping only leading terms results in the expression for the velocity outside the Ekman layer:

$$\mathbf{u} = \frac{1}{H}\left(\mathbf{k}\times\nabla\psi - \frac{h_E}{2H}\nabla\psi\right). \tag{9}$$

Taking curl of (5) and expressing the velocity field in terms of the function of total transports leads to

$$\omega_t + J(\psi, q) + \frac{h_E}{2H}\nabla\psi\cdot\nabla q = -\frac{h_E}{2}q\omega + \nu\nabla^2\omega \quad \text{and} \tag{10}$$

$$\nabla\left(\frac{1}{H}\nabla\psi\right) + \frac{h_E}{2}J\left(\frac{1}{H^2},\psi\right) = \omega, \tag{11}$$

where $q = (2\Omega + \omega)/H$. These equations are valid for arbitrary large variations of depth H, which is essential for the laboratory experiments and also take into account the flow divergence caused by Ekman suction. However, the dominant terms are the same as in the standard quasigeostrophic equations. We retained the evolutionary term in (10) for the sake of generality and to indicate a numerical way of finding steady solutions by the method of equilibration. The system in (10) and (11) will accurately describe transient motions only if the Rossby radius of deformation $L_R = (gH_0)^{1/2}/(2\Omega)$ is much larger than the scale of the motion. In the experiments $L_R = 49.5$ cm, thus, suggesting that the western boundary layer–type transient motions will be practically unaffected but that the basin-scale transients will be somewhat modified; however, both are irrelevant for the final steady states. The kinematic boundary conditions become $\psi = 0$ at the solid walls; at the sponges, the total transport is prescribed in accordance to (2):

$$\frac{\partial\psi}{\partial y} = -H(0, y)U_{1,2}(y), \tag{12}$$

with $\psi = -Q$ at the center of the tank. The no-slip condition on the tangential velocity component is easy to implement by virtue of (9).

Similar to the quasigeostrophic case (Pedlosky 1987, chapter 5), the relative magnitude of the three scales determine the structure of the western boundary current. Balancing the topographic β effect against the bottom drag in (10) gives the Stommel boundary layer thickness L_S:

$$\psi_x\left(\frac{2\Omega}{H}\right)_y \sim \frac{h_E}{2}\frac{2\Omega}{H_0}\frac{1}{H_0}\psi_{xx} \rightarrow L_s = \frac{1}{2S}\left(\frac{\nu}{\Omega}\right)^{1/2}, \tag{13}$$

balancing the topographic β effect against the lateral friction gives the Munk boundary layer thickness L_M:

$$\psi_x\left(\frac{2\Omega}{H}\right)_y \sim \nu\frac{1}{H_0}\psi_{xxxx} \rightarrow L_M = \left(\frac{H_0\nu}{2S\Omega}\right)^{1/3}, \tag{14}$$

and balancing the topographic β effect against the advection of relative vorticity gives the inertial boundary layer thickness L_I:

$$\psi_x\left(\frac{2\Omega}{H}\right)_y \sim \psi_y\frac{1}{H_0}\omega_x \rightarrow L_I = \left(\frac{Q}{2S\Omega R}\right)^{1/2}. \tag{15}$$

In the experiments both L_S and L_M were fixed at about 1.0 cm while L_I varied with Q; $L_I = 1.0$ cm for $Q = 5$ cm^3 s^{-1}.

4. Results of the experiments with varying flow rate

To study dependence of steady flow on parameters we conducted a series of laboratory experiments with fixed gap width $2a = 9.3$ and 14.0 cm and a varyied pumping rate Q in the range from 0 to 60 cm^3 s^{-1}. For the gap width 9.3 cm we saw almost monotonic transition from the penetrating (small Q) to gap-leaping (large Q) flow patterns near $Q = 12$ cm^3 s^{-1} with some evidence of multiple states, but the difference was difficult to distinguish. However, for the gap width 14.0 cm we obtained dramatic evidence of multiple steady states and hysteresis in the range $23 \le Q \le 55$ (cm^3 s^{-1}), which is illustrated in Fig. 2.

Because of a hysteresis we distinguished experiments with increasing and decreasing Q. In the increasing flow rate experiments, a 30-min spinup with the pump switched off led to a solid body rotation state; the spinup time scale was $T_S = H_0/(h_E\Omega) = 100$ s. Then we switched the pump on and gradually increased the flow rate Q in small steps, typically $\Delta Q = 5$ cm^3 s^{-1} (we used smaller $\Delta Q = 1$ cm^3 s^{-1} near the critical values), and let the flow equilibrate to a new state while keeping Q fixed for about 10–15 min, which is sufficiently longer than T_S. Similarly, after the maximum flow rate had been reached and transition to the new state had occurred we started to gradually decrease the flow rate thus tracing a different branch of steady flow patterns. At some reference values of flow rate $Q = 10$, 25, 40, 55, 60 cm^3 s^{-1} we kept Q fixed for an additional 15 min

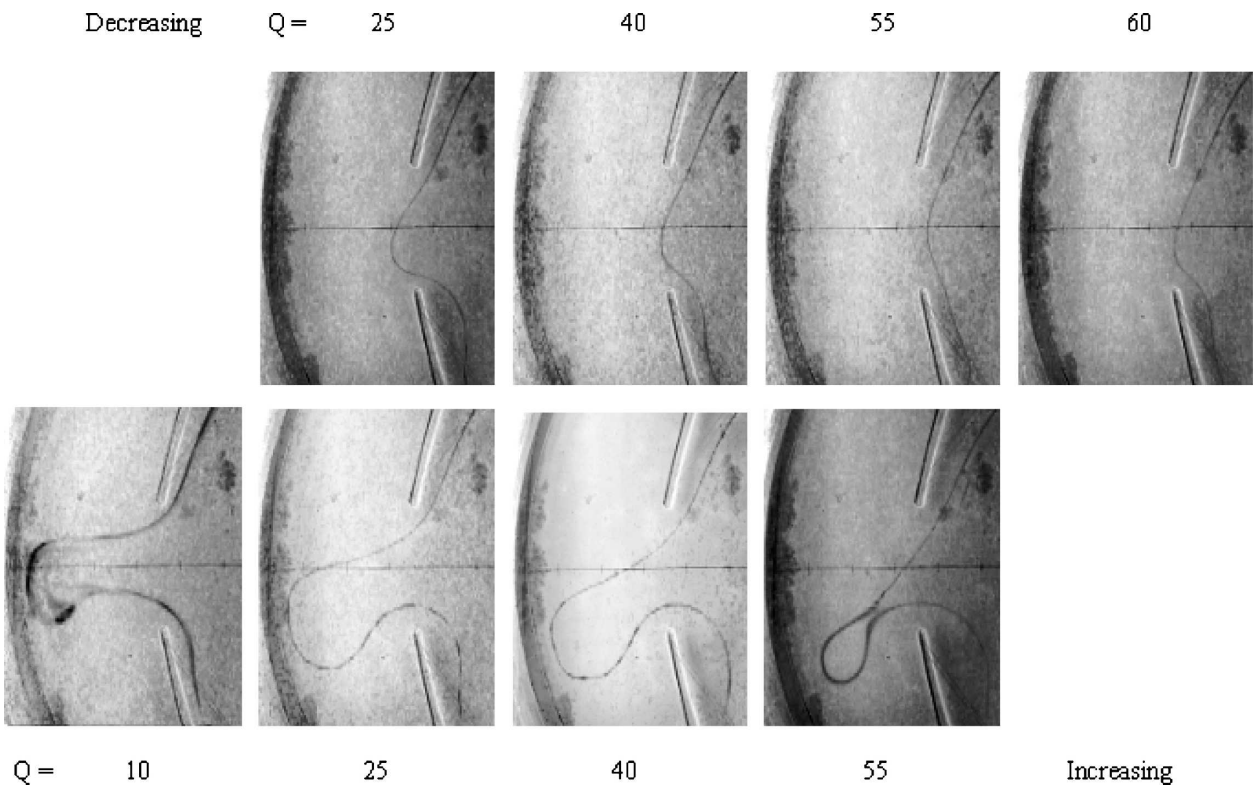

FIG. 2. Steady flow patterns from the laboratory experiments with the gap width of $2a = 14.0$ cm illustrating the hysteresis as the pumping rate Q is varied between 0 and 60 cm^3 s^{-1}. Only a portion of the tank that focused on the gap is shown. A streamline passing through the core of the boundary current is visualized by dye release. The flow is from the top to the bottom of the figure. Within the range $23 \leq Q \leq 55$ (cm^3 s^{-1}) two different steady solutions are possible. Shown are the experiments with (bottom) increasing and (top) decreasing flow rate.

before starting flow visualization using a dye release method. It took approximately another 15 min for the dye to travel across the basin and we also waited to make sure that the streak line was steady. This ensures that the different flow patterns seen in the top versus bottom panels in Fig. 2 represent truly different steady states and not transients.

We note that almost neutrally buoyant dye (food dye mixed with alcohol) was released through a needle in the northern part of the basin. Beyond a short adjustment distance the dye formed a streak and followed a streamline defined by

$$\frac{dx}{u} = \frac{dy}{v} = \text{const.} \tag{16}$$

Because the bottom boundary layer flow is divergent, the streamlines do not coincide with the isolines of total transport in (9) and (8), but for the core of the boundary current, the difference is small. By placing the needle around $x = 0$ and $y = R/2$ we could visualize whether the core of the current leaped across the gap or not.

We also obtained steady numerical solutions for the same values of a and Q. Some important details of the numerical model are given in the appendix. The patterns of the total transport ψ are shown in Fig. 3 using the same arrangement of images. Like in the laboratory experiments we had to trace different branches of steady solutions by increasing or decreasing Q. The numerical model predicts that two different steady solutions are possible within the range $25 \leq Q \leq 52$ (cm^3 s^{-1}). These values are just slightly off from those obtained from the laboratory data; therefore, the last image in the bottom panel in Fig. 3 corresponds to $Q = 52$ rather than 55 (cm^3 s^{-1}). The small discrepancy could be caused by various uncertainties in the laboratory setup such as small variation in fluid viscosity with temperature, warping of the Plexiglas bottom slightly changing the β effect, and some errors in pumping velocities (about 2% for the Ismatec gear pump). In fact, in the experiment with $Q = 22$ cm^3 s^{-1} we estimated the zonal flow in the Sverdrup interior based on consecutive photographs of dye propagation to be 0.0517 cm s^{-1} while the numerical model predicts it to be 0.0526

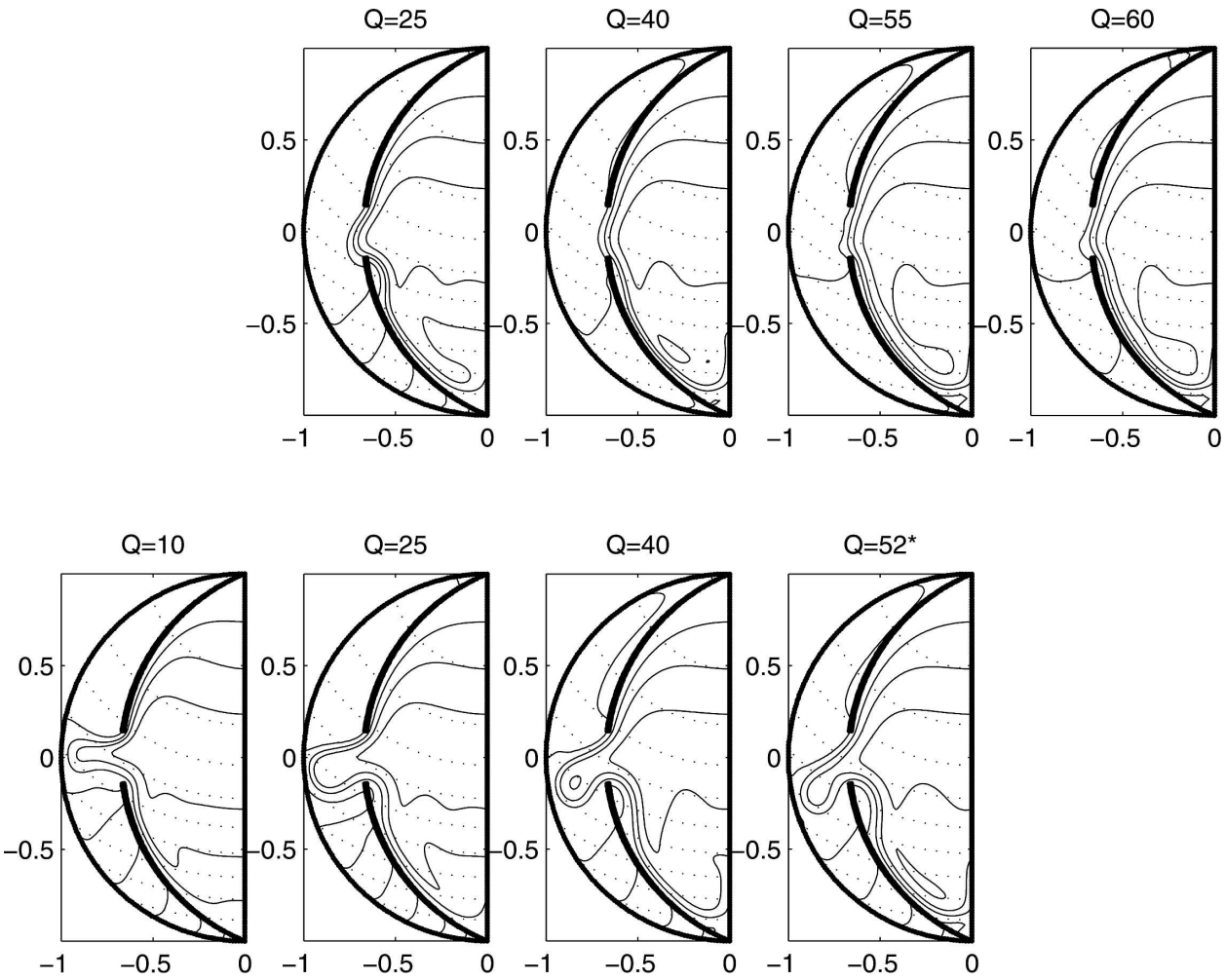

FIG. 3. Steady flow patterns from the numerical solution illustrating the hysteresis as the pumping rate Q is varied. The same parameters as in the laboratory experiments were used. The isolines of the total transport $\psi(x, y)$ are plotted with the contour interval $0.25Q$. The dotted lines indicate geostrophic contours $\Omega/H(x, y) = \text{const}$.

cm s^{-1} according to (2). However, overall, the numerical and laboratory results show very close agreement both in the shape of the loop current and in the critical values of Q between which the multiple states are possible.

According to Sheremet (2001) the two different critical flow rates for which transitions between the gap-penetrating and gap-leaping regimes occur can be explained by dominant term balances in the vicinity of the gap in these two different flow states. The gap-penetrating regime is expected to break down when the width of the penetrating zonal jet L_P becomes comparable to the half-width of the gap a. This follows from the balance between the zonal advection and the β effect [see (19) of Sheremet 2001]. In the present notation

$$L_P = \left(\frac{Q}{H_0\beta}\right)^{1/3} \simeq a, \tag{17}$$

where $\beta = 2\Omega S/H_0$ is the topographic β effect. For the observed critical value $Q = 55$ cm^3 s^{-1}, $L_P = 8.2$ cm; thus, the nondimensional ratio $L_P/a = 1.17$ is as close to unity as expected.

The gap-leaping regime is expected to break when another inertial length scale L_L becomes comparable to a, which follows from balancing the meridional advection and the β effect [see (16) of Sheremet 2001]. In the present notation

$$L_L = \frac{Q}{H_0\beta L_B^2} \simeq a, \tag{18}$$

where L_B is the width of the western boundary current. In (Sheremet 2001) L_B was the Munk thickness L_M; in the present case the width of the western boundary current is determined by a combination of L_M, L_S, and L_I defined in (14), (13), and (15), respectively. If we as-

sume that roughly $L_B = L_M + L_S + L_I$, for the critical we get $Q = 23$ cm^3 s^{-1} and $L_L = 13$ cm and the ratio is $L_L/a = 1.9$.

Equations (17) and (18) should be understood only as scaling estimates. However, they suggest different dependence on the flow rate Q: the power of ⅓ versus 1. This explains the divergence between the critical values of Q as the gap width is increased: they should grow as $\sim a^3$ and $\sim a$, respectively. That is why in the experiments with the gap width $2a = 9.3$ cm, the hysteresis was hardly seen with critical values close to 12 cm^3 s^{-1} while for larger gap width $2a = 14.0$ cm the hysteresis was very dramatic, with multiple flow patterns existing within $23 \le Q \le 55$ (cm^3 s^{-1}). Thus, the experimental results are consistent with these scaling laws.

5. Conclusions

Both the laboratory and numerical experiments presented in this paper dramatically show the existence of multiple states and hysteresis in the gap-leaping problem. The dominant variation in the flow pattern is concentrated near the gap while the upstream and downstream conditions are almost not affected. This indicates that it is the differences in separation and reattachment near the gap that lead to the multiple states similar to Sheremet (2001). Such behavior is well known, there are many examples of multiple states and hysteresis in fluid dynamics: flow past a wing, flow past a veer (Coanda effect), flow past a cavity; however, it is the first laboratory example where the β effect is the crucial player. Without the β effect no westward intensification (Sverdrup 1947; Stommel 1948) occurs and no western boundary current forms. The flow goes from the source to sink as a broad current without entering the gap at all. The idealized geometry of the present problem makes it an excellent test case for numerical models having geophysical applications. The laboratory results also warrant a more scrutinized search for the observational evidence of multiple states and hysteresis in strait flows.

Acknowledgments. This work was generously supported by the Office of Naval Research Grant N00014-02-1-0472 and by the National Science Foundation Grant OCE-0351518. We thank two anonymous reviewers for their valuable comments.

APPENDIX

Numerical Model

To obtain an accurate numerical solution it is always desirable that the domain boundaries coincide with coordinate lines. For this reason we choose a bipolar curvilinear coordinate system consisting of two sets of mutually orthogonal circles. We construct the coordinates appropriate to our case in three steps. First we notice that a conformal mapping

$$x + iy = \tan\left(\frac{\sigma + i\tau}{2}\right) \tag{A1}$$

transforms the interior of a unit circle (corresponding to the perimeter of the tank if we use R to nondimensionalize the horizontal scales) in the complex plane (x, y) into an infinite strip $(-\pi/2 < \sigma < \pi/2, -\infty < \tau < \infty)$ in the complex plane (σ, τ). The circular ridge is then transformed into a line $\sigma = \text{const}$. In terms of real functions the transformation is

$$x = \sin\sigma/(\cos\sigma + \cosh\tau) \quad \text{and} \tag{A2}$$

$$y = \sinh\tau/(\cos\sigma + \cosh\tau). \tag{A3}$$

However, a numerical grid based on this conformal mapping is not convenient because it has higher density of nodes near the Poles $(x = 0, y = -1)$ and $(x = 0, y = 1)$ where it is not needed. Therefore, in the second step we stretch individual variables:

$$\sigma = 2\arctan(\xi) \quad \text{and} \tag{A4}$$

$$\tau = \operatorname{arctanh}\left[\sin\left(\frac{\pi}{2}\eta\right)\right]. \tag{A5}$$

The unit circle in (x, y) becomes a square $-1 < \xi < 1$, $-1 < \eta < 1$. A uniform grid in (ξ, η) will have a uniform step in x along $y = 0$ due to (A4) and will have a uniform step in ϕ along the circumference $r = 1$ due to (A5), where $x + iy = r\exp(i\phi)$ (see Fig. A1). The ridge will be located at $\xi = -⅔$. Further stretching can be applied in the third step: $\xi = \xi(\xi')$, $\eta = \eta(\eta')$ if one desires increased resolution near the ridge or the boundaries. An example of such stretching can be found in Sheremet (2001). Another option is to use stretching based on the collocation points of Chebyshev polynomials. Here for simplicity we omit that step. The Lamé coefficients of the orthogonal curvilinear system (ξ, η) are

$$h_\xi = h\frac{d\sigma}{d\xi} = h\left[2\cos^2\left(\frac{\sigma}{2}\right)\right] \quad \text{and} \tag{A6}$$

$$h_\eta = h\frac{d\tau}{d\eta} = h\cosh^2(\tau)\cos\left(\frac{\pi}{2}\eta\right)\frac{\pi}{2}, \tag{A7}$$

where h is the scalar factor of the conformal mapping (A1):

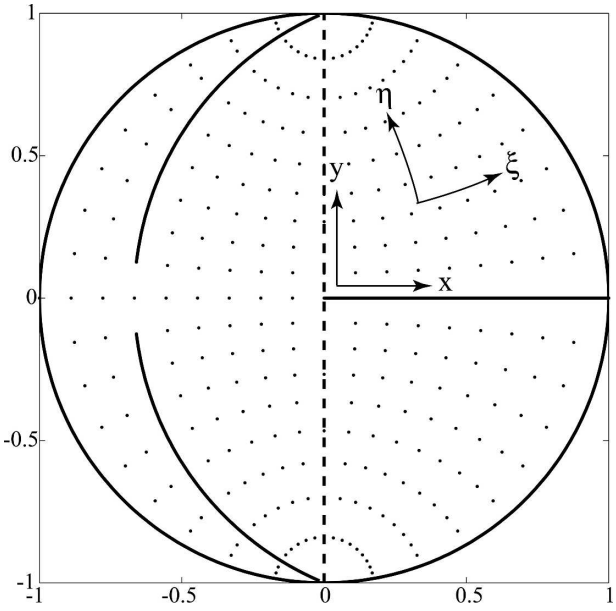

FIG. A1. Bipolar orthogonal curvilinear coordinates (ξ, η) used to accommodate circular boundaries and the ridge. Dots indicate the nodes of a grid dividing a unit square in the (ξ, η) space into 18×18 uniform cells.

$$h = \left|\frac{d(x + iy)}{d(\sigma + i\tau)}\right| = (\cos\sigma + \cosh\tau)^{-1}, \qquad \text{(A8)}$$

and σ and τ should be expressed in terms of ξ and η according to (A4) and (A5).

The expressions for the differential operators present in the system of equations in (10) and (11) in a general orthogonal curvilinear coordinate system can be found, for example, in Batchelor (2000, his appendix 2). We approximate all terms in the equations using standard centered differences on a uniform grid with $N_\xi \times N_\eta$ cells covering the region $-1 < \xi < 0$, $-1 < \eta < 1$. We used a grid (90×190) for most of the calculations and checked convergence by conducting selected calculations on a (180×380) grid. Steady solutions were obtained by the method of equilibration (as the limiting solutions at large time).

REFERENCES

Batchelor, G. K., 2000: *An Introduction to Fluid Dynamics*. Cambridge University Press, 615 pp.

Cho, Y.-K., R. C. Beardsley, and V. A. Sheremet, 2002: On the cause of Scotian Shelf Water crossovers. *Geophys. Res. Lett.,* **29,** 2212, doi:10.1029/2002GL014968.

Ekman, V. W., 1905: On the influence of the earth's rotation on ocean-currents. *Ark. Mat. Astr. Fys.,* **2** (11), 1–52.

Gromeka, I. S., 1885: On vortex motions of a liquid on sphere (in Russian). *Uch. Zap. Imp. Kazan. Univ.,* Vol. III, 35 pp. [Reprinted in *Gromeka, I. S., Collected papers,* Academy of Science USSR, Moscow, 1952, 183–205.]

Johnson, E. R., and N. R. McDonald, 2004: The motion of a vortex near a gap in the wall. *Phys. Fluids,* **16,** 462–469.

Nof, D., and D. Olson, 1983: On the flow through broad gaps with application to the windward passage. *J. Phys. Oceanogr.,* **13,** 1940–1956.

Pedlosky, J., 1968: An overlooked aspect of the wind-driven oceanic circulation. *J. Fluid Mech.,* **32,** 809–821.

——, 1987: *Geophysical Fluid Dynamics*. 2d ed. Springer-Verlag, 710 pp.

——, and H. P. Greenspan, 1967: A simple laboratory model for the oceanic circulation. *J. Fluid Mech.,* **27,** 291–304.

Sheremet, V. A., 2001: Hysteresis of a western boundary current leaping across a gap. *J. Phys. Oceanogr.,* **31,** 1247–1259.

Simmons, H. L., and D. Nof, 2002: The squeezing of eddies through gaps. *J. Phys. Oceanogr.,* **32,** 314–335.

Stommel, H., 1948: The westward intensification of wind-driven ocean currents. *Eos, Trans. Amer. Geophys. Union,* **29,** 202–206.

Sverdrup, H., 1947: Wind-driven currents in a baroclinic ocean: With application to the equatorial currents of the eastern Pacific. *Proc. Natl. Acad. Sci. USA,* **33,** 318–326.

Toole, J. M., R. C. Millard, Z. Wang, and S. Pu, 1990: Observations of the Pacific North Equatorial Current bifurcation at the Philippine coast. *J. Phys. Oceanogr.,* **20,** 307–318.

Zavala Sanson, L., and G. J. F. van Heijst, 2002: Ekman effects in a rotating flow over bottom topography. *J. Fluid Mech.,* **471,** 239–255.